Scientific Research Publishing

Journal of Signal and Information Processing, 2025, 16(4), 45-57
https://www.scirp.org/journal/jsip
ISSN Online: 2159-4481
ISSN Print: 2159-4465

An Iterative Reconstruction Algorithm Based on Detail Transfer for Few-View Computed Tomography

Jing Huang, Lisha Wu, Dongjiang Ji*

School of Science, Tianjin University of Technology and Education, Tianjin, China
Email: *zjkjdj@tute.edu.cn

How to cite this paper: Huang, J., Wu, L.S. and Ji, D.J. (2025) An Iterative Reconstruction Algorithm Based on Detail Transfer for Few-View Computed Tomography. *Journal of Signal and Information Processing*, **16**, 45-57.
https://doi.org/10.4236/jsip.2025.164004

Received: September 9, 2025
Accepted: October 13, 2025
Published: October 16, 2025

Abstract

Computed Tomography (CT) is widely used in medical diagnosis. Filtered Back Projection (FBP), a traditional analytical method, is commonly used in clinical CT to preserve high-frequency details but introduces streak artifacts in few-view data. In contrast, iterative reconstruction algorithms improve image quality by incorporating accurate models of imaging physics and noise. However, they often require explicit regularization or specialized network architectures, leading to complex optimization challenges. This paper proposes an iterative reconstruction algorithm based on detail transfer (DT), which requires the prior detail information extracted from the FBP-reconstructed image. Specifically, the detail information extracted from the FBP-reconstructed image is combined with the SART reconstruction results using mask-allocated weights to generate the initial value for the iterative reconstruction process. During the iterations, as characteristics of iterative algorithm, the low-frequency information is restored first and high-frequency information is gradually recovered, the extracted detail information is weighted with the iteratively reconstructed image to accelerate the restoration of high-frequency information. This approach speeds up the convergence of the algorithm. The iterative reconstruction algorithm adopts the Simultaneous Algebraic Reconstruction Technique (SART), and thus, the proposed method is referred to as SART-DT. Experimental results show that SART-DT effectively removes artifacts and restores details, offering superior reconstruction quality and better preservation of fine details compared to other methods.

Keywords

CT Reconstruction, Detail Transfer, FBP, SART

1. Introduction

With the development of medical imaging technology, computed tomography (CT) has become an indispensable tool in diagnosis and treatment planning. The quality of CT images directly affects the detection, classification and treatment results of diseases. Image reconstruction is a key step in the CT imaging process, and it is responsible for recovering high-resolution and high-contrast images from the projection data collected by the detector.

There are two major classes of reconstruction algorithms: analytical and iterative. In 1917, Radon proposed the Radon transform, which is the mathematical basis for analytical reconstruction [1]. It maps a two-dimensional function to a one-dimensional function and describes the properties of line integrals of objects from different angles. The inverse transformation of the Radon transform provides the theoretical basis for recovering the original image from the projection data. Analytical algorithms are one of the earliest used CT reconstruction methods, among which Filtered Back Projection (FBP) [2] has been widely used in medical and industrial CT scanners due to its ability to generate CT studies of adequate image quality in a robust and fast manner. The FBP algorithm utilizes the properties of the Fourier transform to reconstruct the image from the projection data through a back-projection step, which means that it does not require complex iterative calculations to approximate the solution, thus saving a lot of computing time. With the development of technology, the iterative reconstruction algorithm has been paid more attention. Iterative algorithm can improve image quality by approaching the optimal solution step by step, especially in the processing of noisy data or low-dose imaging [3]. The development of iterative Reconstruction algorithm can be traced back to the Algebraic Reconstruction Technique (ART) proposed by Gordon R [4] *et al.* The SART algorithm proposed by A. H. Anderson and A. C. Kak [5] in 1984 is an improved iterative reconstruction algorithm, which requires only a small number of iterations to obtain good reconstruction quality and accuracy. This method uses the errors of all rays of a pixel under the same projection Angle to determine the correction of the pixel, rather than only considering one ray. It maintains the advantages of simple structure and easy implementation of ART algorithm, while improving the convergence speed and stability of the algorithm, and it has a wide range of applications [6] [7]. Hybrid Iterative Reconstruction (HIR) [8] [9] combines iterative processing of original data domain and image domain to reduce artifacts and noise and improve image quality. These algorithms typically use a back projection step followed by iterative filtering of the image data. Based on the traditional Iterative Reconstruction algorithm, Model-Based Iterative Reconstruction (MBIR) [10] introduces more complex and accurate models, including physical models, noise models and prior models, to improve image quality, reduce noise and artifacts [11]. It can still maintain high image quality under low dose conditions, which is suitable for radiation dose control in clinical applications. However, due to the introduction of complex physical model and noise model, the computation is large and high

performance computing resources are required. With the rapid development of deep learning technology, convolutional neural network-based methods have been widely used in various fields and achieved excellent results. Due to its superior performance, researchers have introduced it into the field of CT image reconstruction [12] [13].

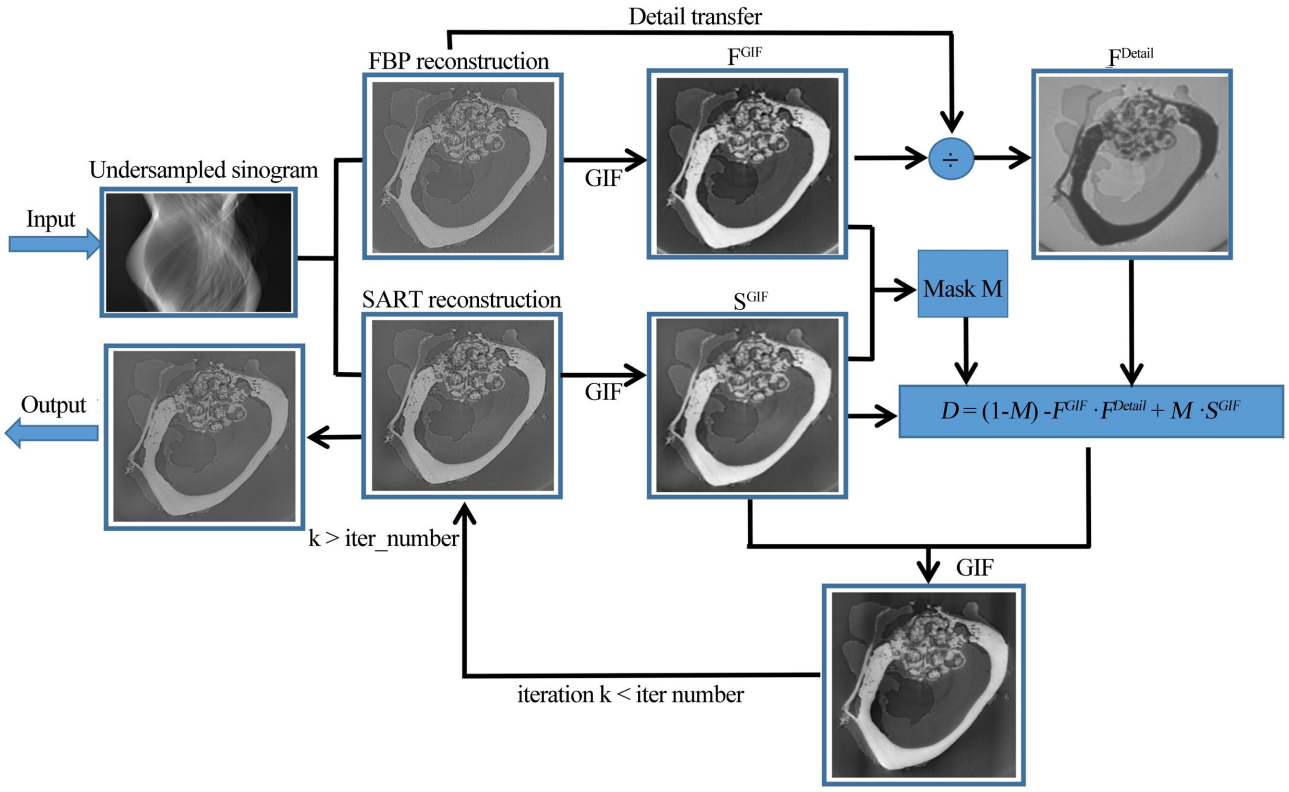

Figure 1. The workflow of the SART-DT algorithm.

To facilitate radiation dose reduction while maintaining diagnostic information and image quality, one category of reconstruction algorithm for few-view CT is iterative reconstruction algorithm. Compared with the FBP algorithm, iterative CT reconstruction methods are able to model projection noise or utilize prior knowledge to reduce noise or artifacts. However, although the FBP method is affected by noise, the reconstructed image also contains detailed information of the reconstructed object. Therefore, it is necessary to maintain the important information in the FBP reconstructed image while suppressing noise. The recently proposed guided filtering method [14] can achieve good noise reduction effect and noise reduction quality at the same time. SART gradually adjusts the image to match the projection data, and gradually approaches the real image through multiple iterations. In the initial iteration of SART, the low-frequency information of image is mainly recovered. This is because the initial iterations focus on adjusting the general structure and shape to match the projection data. As the number of iterations increases, detailed information is gradually restored, and high-frequency components

in the image, such as edges and small structures, become clearer. To this end, this article proposes a new reconstruction method called Simultaneous Algebraic Reconstruction Technique-Detail Transfer (SART-DT). In order to retain more image detail features, this method passes the high-frequency detail information in the FBP reconstructed image to the subsequent SART process [15]. First, FBP and SART reconstruction are performed on the projection data respectively, and a detail layer is calculated from the FBP reconstructed image, which is passed to the SART iteration process, and iterates continuously until the final reconstructed image is obtained. The flowchart of this method is shown in **Figure 1**.

The structure of this work is as follows: Section 2 provides the related algorithm of our work and Section 3 introduces the theory and process of our proposed method. The experiments and their results are reported in Section 4. Finally, Section 5 discusses and concludes this work.

2. Related Methods

2.1. FBP Reconstructed Algorithm

Filtered back projection (FBP) [2] is a spatial processing technique based on Fourier transform. Firstly, the projection data were filtered to remove noise and improve image quality. Then the backprojection operation was carried out, that is, the value of each pixel was assigned to the detector under the corresponding projection Angle. Finally, the back projection results were superimposed to obtain the reconstructed CT images. It is characterized by convolutional processing of the projections under each acquisition projection Angle before back projection, thus improving the shape artifacts caused by the point spread function, and the reconstructed image quality is better. Despite its overall acceptable performance, CT studies that are reconstructed with FBP can be affected by high image noise, artifacts (e.g. streak artifacts), or poor low-contrast detectability in specific clinical scenarios.

2.2. Guided Image Filtering

GIF is a local linear filter with good edge preservation and low time complexity. In GIF, the filtered output f^{GIF} is a linear transformation of the guidance image I into a square window ω_n with pixel n as the center and radius r [14]:

$$f_i^{GIF} = a_n I_i + b_n \quad \forall i \in \omega_n \tag{1}$$

where i is pixel index. (a_n, b_n) are linear coefficients assumed to be constant in ω_n. In this work, the size of ω_n is 3 × 3. The (a_n, b_n) are determined by minimizing the following cost function in ω_n:

$$E(a_n, b_n) = \sum_{i \in \omega_n} \left(\left(a_n I_i + b_n - f_i \right)^2 + \varepsilon a_n^2 \right) \tag{2}$$

where ε is a regularization parameter that penalizes large a_n values. f_i is the filtering input of image f at pixel i.

Equation (2) represents the linear ridge regression model, and its solution can

be expressed by the linear regression:

$$a_n = \frac{\frac{1}{|\omega|}\sum_{i\in\omega_n} f_i I_i - \overline{f}_n \mu_n}{\sigma_n^2 + \varepsilon} \tag{3}$$

$$b_n = \overline{f}_n - a_n \mu_n \tag{4}$$

where μ_n and σ_n^2 are the mean value and variance of the guidance image I in ω_n, respectively. f_n is the mean value of input image f in ω_n. $|\omega|$ is the number of pixels in ω_n. If the guidance image I is set to the filtering input image f. We can obtain:

$$a_n = \frac{\sigma_n^2}{\sigma_n^2 + \varepsilon} \tag{5}$$

$$b_n = (1 - a_n)\mu_n \tag{6}$$

Because a given pixel i is involved in several windows, the values of J_i are not identical when computed in different windows. A simple strategy is to average all values of f_i^{GIF}. After computing (a_n, b_n) for all windows, the output of the filter can be computed as:

$$f_i^{GIF} = \frac{1}{|\omega|}\sum_{n\in\omega_n}(a_n I_i + b_n) = \overline{a}_n I_i + \overline{b}_n \tag{7}$$

where $\overline{a}_n = 1/|\omega|\sum_{n\in\omega_i} a_n$ and $\overline{b}_n = 1/|\omega|\sum_{n\in\omega_i} b_n$ are the average coefficients calculated from all windows overlapping i.

2.3. SART Reconstructed Algorithm

A CT imaging system can be modeled as:

$$Af = p \tag{8}$$

where $A = (a_{ij})$ denotes an $M \times N$ measurement matrix, a_{ij} is the contribution of the j^{th} pixel to the i^{th} X-ray, p is the projection data collected by the detector, and $f \in R^N$ is the linear attenuation coefficients of the measured object. The task of CT imaging is to reconstruct f from p.

The convergence of the following simultaneous iterative scheme is considered [16] [17]:

$$f^{(K+1)} = f^{(K)} + \lambda_K V^{-1} A^* W\left(p - Af^{(K)}\right) \tag{9}$$

where $K = 0,1\ldots, \lambda_K > 0$ is the relaxation coefficient, V and W are two positive definite diagonal matrices of order N and M.

The SART algorithm is a special case of Equation (9), and its formula can be expressed as [5]:

$$f_j^{(K+1)} = f_j^{(K)} + \frac{\lambda_K}{\sum_{i=1}^{M} a_{ij}} \sum_{i=1}^{M} \left[\frac{p_i - \sum_{n=1}^{N} a_{in} f_n^{(K)}}{\sum_{n=1}^{N} a_{in}} \right] a_{ij} \tag{10}$$

with V and W defined:

$$V = \mathrm{diag}\left(V^1, V^2, \ldots, V^N\right) \tag{11}$$

$$W = \mathrm{diag}\left(W^1, W^2, \ldots, W^M\right) \tag{12}$$

and with

$$V^j = \sum_{i=1}^{M} a_{ij}, \text{ for j } = 1, \ldots, N \tag{13}$$

$$\frac{1}{W^i} = \sum_{n=1}^{N} a_{in}, \text{ for } i = 1, \ldots, M \tag{14}$$

The SART relaxation parameter λ_K was chosen by considering the convergence theorem [18]: Theorem 1: Assuming that $W^i > 0$ for all $i = 1, 2, \ldots M$, and if, for all $K \geq 0$,

$$0 \leq \varepsilon \leq \lambda_K \leq (2 - \varepsilon) \Big/ \max\left\{W^i \,|\, i = 1, 2, \ldots, M\right\} \tag{15}$$

where ε is an arbitrarily small constant, then any sequence $\left\{f^{(K)}\right\}_{K=0}^{\infty}$ generated by SART converges to the weighted least-squares solution $f^* = \arg\min\left\{\|Af - p\|_2 \,\middle|\, f \in R^n\right\}$.

3. SART-DT Algorithm

The algorithm proposed in this work is to induce the detail information reconstructed by FBP algorithm to the initial iteration of SART, in order to accelerate the convergence speed and improve the quality of the reconstructed image.

3.1. Mask M

In order to generate a better SART iterative initial value, we calculate a Mask M and get the guided image D by the following formula:

$$D = (1 - M) \cdot F^{GIF} + M \cdot f^{(K+1)GIF} \tag{16}$$

where F denotes the FBP reconstructed image, F^{GIF} is computed using the guided image filtering on F. For convenience, S is represented as SART reconstruction image, and we use S^{GIF} to represent $f^{(K+1)GIF}$. In such a way, M adjusts the relative contribution of information from different sources during the generation of initial values in the expectation of obtaining better initial values and thus improving the quality of reconstructed images in the subsequent iterative reconstruction process. We add a threshold to compute M by looking for pixels with a small difference between F^{GIF} and S^{GIF}:

$$M^{Shad} = \begin{cases} 1 & when\ F_{Lin}^{GIF} - S_{Lin}^{GIF} \leq \tau_{shad} \\ 0 & otherwise. \end{cases} \tag{17}$$

where F_{Lin}^{GIF} and S_{Lin}^{GIF} are linearized versions of the corresponding F^{GIF} and S^{GIF}. The SART algorithm is used to iterate over the initial values to obtain the final reconstructed image.

3.2. Detail Information Transfer

While the GIF can reduce noise, it cannot add detail information that may be present in the FBP reconstructed image. To transfer the detail information we begin by computing a detail layer from the FBP reconstructed image as the following ratio:

$$F^{Detail} = \frac{F+\varepsilon}{F^{GIF}+\varepsilon} \tag{18}$$

The ratio captures the local detail variation in F and is commonly called a quotient image [19] or ratio image [20] in computer vision. **Figure 2** shows that the advantage of using the GIF to rather than a classic low-pass Gaussian filter is that the haloing was reduced.

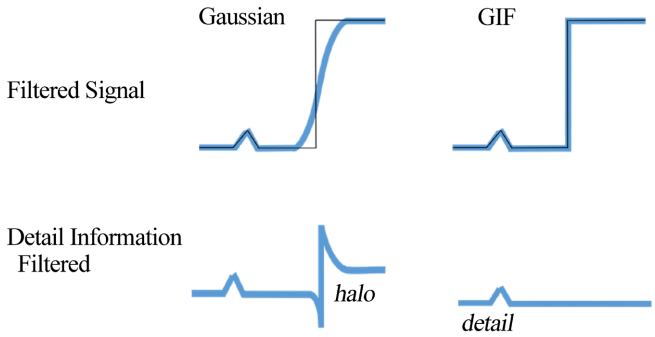

Figure 2. (left) A Gaussian low-pass filter blurs across all edges and will therefore create strong peaks and valleys in the detail image that cause halos. (right) The GIF does not smooth across strong edges and thereby reduces halos, while still capturing detail.

Although the FBP reconstructed image contains detail information, it also contains noise that may lead to transfer spurious detail. Therefore, ε was added to both the numerator and denominator of the Equation (19) to reject transfer the noise and also avoid division by zero. In this work, $\varepsilon = 9\times10^{-5}$ and $\varepsilon = 9\times10^{-7}$ were used in simulation experiment. To transfer the detail information, the final image D is computed as:

$$D = (1-M)\cdot F^{GIF}\cdot F^{Detail} + M\cdot f^{(K+1)GIF} \tag{19}$$

3.3. Algorithm Process

In the process of our proposed method, the results obtained by FBP reconstruction and SART reconstruction of projection data are denoted as F and S. Then F and S are filtered by the guided image, respectively, to obtain the corresponding results F^{GIF} and S^{GIF}. In order to better retain and transmit the detail information to improve the delicacy and accuracy of the reconstructed image, the detail information F^{Detail} is calculated from F through Equation (18). In order to provide a better initial value for the following SART reconstruction, this detail layer is transferred to F^{GIF} and combined with S^{GIF} to obtain the final image D as shown in Equation (19). In the process of obtaining the initial

value, Mask calculated by Equation (17) is used as a weight, controlling the contribution of the information extracted from two different sources F^{GIF} and S^{GIF} in the initial value. Then D is as the guidance image to filter the image S^{GIF}, and the obtained image $L^{GIF}\left(S^{GIF}\right)$:

$$L_i^{GIF}\left(f^{(K+1)GIF}\right) = a_n D_i + b_n \qquad \forall i \in \omega_n \tag{20}$$

where $f^{(K+1)GIF}$ is S^{GIF}. And $L^{GIF}\left(f^{(K+1)GIF}\right)$ denotes the image $f^{(K+1)GIF}$ after GIF. i is pixel index, (a_n, b_n) are linear coefficients assumed to be constant in square window ω_n which centered at pixel n.

$L_i^{GIF}\left(f^{(K+1)GIF}\right)$ is used as the initial value of SRAT iteration to participate in the following SART reconstruction process for iteration until the final image is obtained.

To explain the SART-DT algorithm more clearly, the corresponding pseudocode is presented, as illustrated in Algorithm 1.

Algorithm 1. Pseudocode for SART-DT algorithm.

Input: Undersampled sonogram, the SART relaxation parameter λ_K, the SART iteration initial value $f^{(0)} = 0$, the number of iterations M_{iter}.

Initialize: $K \leftarrow 0$

1. FBP reconstruction: F
2. FBP reconstructed image after guided image filtering: F^{GIF}
3. Get detail layer: $F^{Detail} = \dfrac{F + \varepsilon}{F^{GIF} + \varepsilon}$

While $K < M_{iter}$

4. SART reconstruction by Equation (10): $f^{(K+1)}$
5. Guided image filtering: $f^{(K+1)GIF}$
6. Detail transfer: $D = (1 - M) \cdot F^{GIF} \cdot F^{Detail} + M \cdot f^{(K+1)GIF}$
7. Guided image filtering: $L_i^{GIF}\left(f^{(K+1)GIF}\right) = a_n D_i + b_n$
8. $f^{(K+1)} \leftarrow L^{GIF}\left(f^{(K+1)GIF}\right)$
9. $K \leftarrow K + 1$
10. End while

Output: The reconstructed image using SART-DT algorithm

End

4. Experiment Results

In this study, we use simulation experiments to validate and evaluate the proposed algorithm. There are six comparison algorithms selected in this work, including SART method, FBP method, SART-TV [21], SART- L_0 [22], SART-GIF [23] and FBP-GIF. Among them, the FBP-GIF method refers to performing guided image filtering on the result of each iteration of SART, with the FBP reconstruction result serving as the guided image. The SART-GIF method also performs guided image filtering on the result of each iteration of SART, and the guided image. In order to quantitatively evaluate the reconstruction effect of each comparison algorithm,

structural similarity (SSIM) [24], peak signal-to-noise ratio (PSNR) [25] and mean square error (MSE) [26] are used as evaluation indexes in this work.

In the simulation experiments, the projection data of pigeons are reconstructed by SART-DT method, and the experimental results are compared with those of SART method, FBP method, SART-TV method, SART- L_0 method, FBP-GIF method and SART-GIF method. In order to show the details of the image more clearly, we selected two regions of interest marked with red and green rectangles for the image results, and enlarged them as shown in **Figure 3**. In these local magnification regions, the image reconstruction effect of our proposed algorithm compared with other comparison algorithms can be more clearly observed.

As can be seen from **Figure 3(c)**, the results reconstructed using FBP still have obvious strip artifacts, while the strip artifacts of the image reconstructed by FBP-GIF have been somewhat reduced. As shown in **Figure 3(b)**, by observing the local magnification area of the SART reconstructed image, you can see that there are fewer artifacts but the detailed structure is not clear enough. The results of the SART-TV method can be seen in both local magnification areas, and some detailed information is lost in **Figure 3(d)**. The results of the SART- L_0 method are shown in **Figure 3(e)**. In the green magnified area, the texture of the background is smoothed out, while in the red magnified area, the edges of the image are less clear. In **Figure 3(f)** and **Figure 3(h)**, the reconstructed images of the SART-GIF method and the SART-DT method have similar reconstruction effects from a subjective point of view, the stripe artifacts are obviously suppressed, and the detailed textures are also relatively clear.

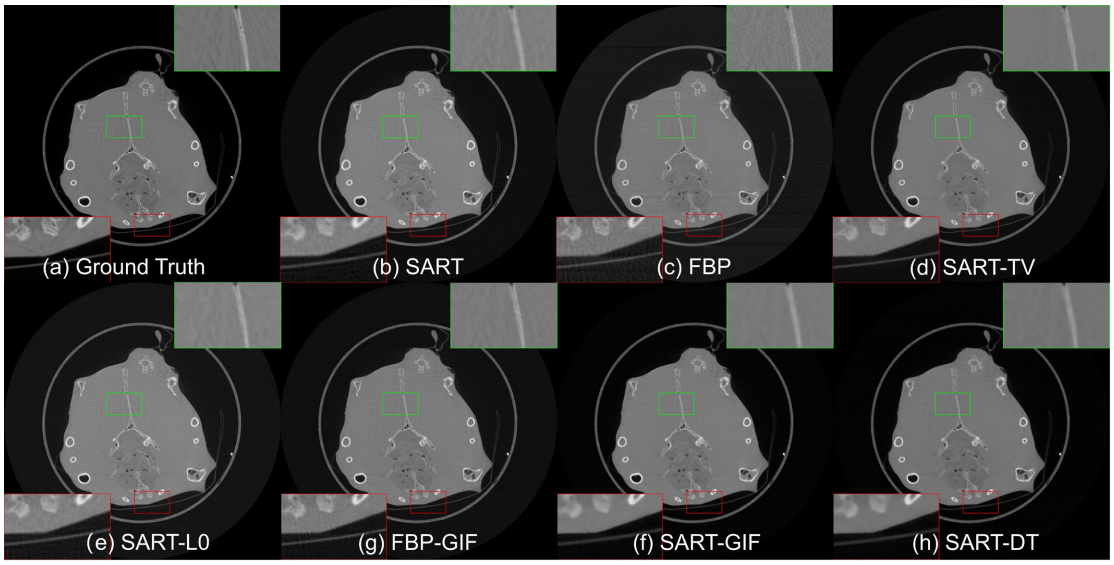

Figure 3. Reconstruction results of simulated projection data under different reconstruction methods.

Table 1 shows the comparison of the reconstruction performance of using various methods. From **Table 1**, it can be clearly seen that the SSIM and PSNR values of the reconstructed images by the SART-DT method are the largest, and the MSE

values are the smallest. That is to say, among the comparison algorithms, the reconstructed image effect of the SART-DT algorithm is the best.

Table 1. The evaluation index values of the results of different reconstruction methods in simulation experiments.

	SART	FBP	SART- L_0	SART-TV	FBP-GIF	SART-GIF	SART-DT
SSIM	0.9340	0.9319	0.8182	0.9695	0.9046	0.9909	0.9949
PSNR (dB)	24.9629	22.3221	22.9646	28.9406	25.2908	31.0849	32.5081
MSE	207.3926	380.9498	328.5676	82.9897	192.3083	50.6507	36.4979

In order to evaluate the reconstruction performance of different methods more intuitively, **Figure 4** shows the relative error results of each method and the ground truth as the number of iterations increases. It can be seen that among all comparison methods, the relative error value of the SART method is the largest at the beginning of the iteration, and decreases significantly with the increase of the number of iterations, but finally converges to about 0.13. The relative errors of SART-GIF and FBP-GIF almost all dropped from 0.56 to around 0.12. The relative error results of the SART- L_0 according to different values of the smoothing parameter λ are shown in **Figure 4(b)**. When λ is 0.0001, the SART- L_0 converges to a higher relative error, and when λ takes other values, it also converges to around 0.12. **Figure 4(c)** is a comparison of the relative error convergence curve of the SART-TV algorithm and the SART-DT method under different smoothing parameters λ. It can be seen from the convergence curve that SART-TV basically converges from 0.56 to 0.12. The relative error value of the SART-DT method is small at the beginning of the iteration, and decreases as the number of iterations increases, and finally converges to about 0.09, which is lower than convergence results of other methods.

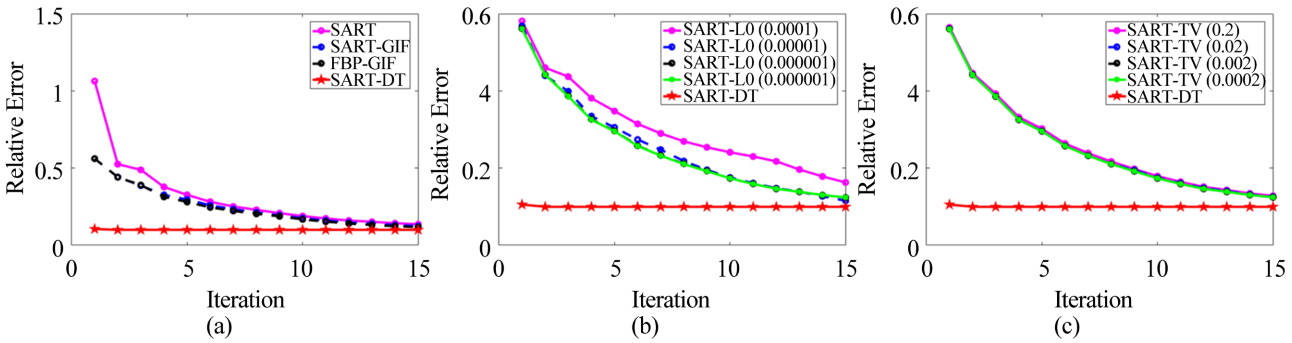

Figure 4. The relative error curve between the results of each iteration of each reconstruction method and GT in the simulation experiment.

5. Conclusion

Few-view image reconstruction remains a significant challenge in CT imaging, particularly when dealing with projection data compromised by noise. The SART-

DT algorithm proposed in this study addresses this challenge by integrating the strengths of the SART algorithm with a detail transfer technique. By introducing a detail layer derived from FBP reconstruction results at the initial stage of the iterative SART process, the algorithm effectively compensates for the inherent limitations of SART in preserving high-frequency information. This enhancement in the reconstruction process not only mitigates striation artifacts but also improves the overall quality and fidelity of the reconstructed images. The experimental results demonstrate the effectiveness of the SART-DT algorithm in producing high-quality reconstructions, making it a promising approach for few-view CT imaging applications.

Conflicts of Interest

The authors declare no conflicts of interest regarding the publication of this paper.

References

[1] Radon, J. (1983) Über die Bestimmung von Funktionen durch ihre Integralwerte längs gewisser Mannigfaltigkeiten. 71-86.

[2] Feldkamp, L.A., Davis, L.C. and Kress, J.W. (1984) Practical Cone-Beam Algorithm. *Journal of the Optical Society of America A*, **1**, 612-619. https://doi.org/10.1364/josaa.1.000612

[3] Flores, L., Vidal, V. and Verdú, G. (2015) Iterative Reconstruction from Few-View Projections. *Procedia Computer Science*, **51**, 703-712. https://doi.org/10.1016/j.procs.2015.05.188

[4] Gordon, R., Bender, R. and Herman, G.T. (1970) Algebraic Reconstruction Techniques (ART) for Three-Dimensional Electron Microscopy and X-Ray Photography. *Journal of Theoretical Biology*, **29**, 471-481. https://doi.org/10.1016/0022-5193(70)90109-8

[5] Andersen, A. (1984) Simultaneous Algebraic Reconstruction Technique (SART): A Superior Implementation of the ART Algorithm. *Ultrasonic Imaging*, **6**, 81-94. https://doi.org/10.1016/0161-7346(84)90008-7

[6] Chen, Y., Lu, Y., Ma, X. and Xu, Y. (2022) A Content-Adaptive Unstructured Grid Based Regularized CT Reconstruction Method with a SART-Type Preconditioned Fixed-Point Proximity Algorithm. *Inverse Problems*, **38**, Article ID: 035005. https://doi.org/10.1088/1361-6420/ac490f

[7] Chee, G., O'Connell, D., Yang, Y.M., Singhrao, K., Low, D.A. and Lewis, J.H. (2019) McSART: An Iterative Model-Based, Motion-Compensated SART Algorithm for CBCT Reconstruction. *Physics in Medicine & Biology*, **64**, Article ID: 095013. https://doi.org/10.1088/1361-6560/ab07d6

[8] Greffier, J., Frandon, J., Larbi, A., Beregi, J.P. and Pereira, F. (2019) CT Iterative Reconstruction Algorithms: A Task-Based Image Quality Assessment. *European Radiology*, **30**, 487-500. https://doi.org/10.1007/s00330-019-06359-6

[9] Stiller, W. (2018) Basics of Iterative Reconstruction Methods in Computed Tomography: A Vendor-Independent Overview. *European Journal of Radiology*, **109**, 147-154. https://doi.org/10.1016/j.ejrad.2018.10.025

[10] Huang, Z., Ye, S., McCann, M.T. and Ravishankar, S. (2023) Model-Based Reconstruction with Learning: From Unsupervised to Supervised and Beyond. In: Ye, J.C.,

Eldar, Y.C. and Unser, M., Eds., *Deep Learning for Biomedical Image Reconstruction*, Cambridge University Press, 28-52. https://doi.org/10.1017/9781009042529.005

[11] Kumar, D., Parkinson, D.Y. and Donatelli, J.J. (2024) tomoCAM: Fast Model-Based Iterative Reconstruction via GPU Acceleration and Non-Uniform Fast Fourier Transforms. *Journal of Synchrotron Radiation*, **31**, 85-94. https://doi.org/10.1107/s1600577523008962

[12] Song, B., Shen, L. and Xing, L. (2023) PINER: Prior-Informed Implicit Neural Representation Learning for Test-Time Adaptation in Sparse-View CT Reconstruction. 2023 *IEEE/CVF Winter Conference on Applications of Computer Vision* (*WACV*), Waikoloa, 2-7 January 2023, 1928-1937. https://doi.org/10.1109/wacv56688.2023.00197

[13] Lei, J. and Liu, Q.B. (2022) Semi-Supervised Learning-Assisted Imaging Method for Electrical Capacitance Tomography. *Applied Mathematical Modelling*, **106**, 126-149. https://doi.org/10.1016/j.apm.2022.01.027

[14] He, K., Sun, J. and Tang, X. (2013) Guided Image Filtering. *IEEE Transactions on Pattern Analysis and Machine Intelligence*, **35**, 1397-1409. https://doi.org/10.1109/tpami.2012.213

[15] Petschnigg, G., Szeliski, R., Agrawala, M., Cohen, M., Hoppe, H. and Toyama, K. (2004) Digital Photography with Flash and No-Flash Image Pairs. *ACM Transactions on Graphics*, **23**, 664-672. https://doi.org/10.1145/1015706.1015777

[16] Qu, G., Wang, C. and Jiang, M. (2009) Necessary and Sufficient Convergence Conditions for Algebraic Image Reconstruction Algorithms. *IEEE Transactions on Image Processing*, **18**, 435-440. https://doi.org/10.1109/tip.2008.2008076

[17] Han, G., Qu, G. and Jiang, M. (2016) Relaxation Strategy for the Landweber Method. *Signal Processing*, **125**, 87-96. https://doi.org/10.1016/j.sigpro.2016.01.010

[18] Censor, Y., Elfving, T., Herman, G.T. and Nikazad, T. (2008) On Diagonally Relaxed Orthogonal Projection Methods. *SIAM Journal on Scientific Computing*, **30**, 473-504. https://doi.org/10.1137/050639399

[19] Shashua, A. and Riklin-Raviv, T. (2001) The Quotient Image: Class-Based Re-Rendering and Recognition with Varying Illuminations. *IEEE Transactions on Pattern Analysis and Machine Intelligence*, **23**, 129-139. https://doi.org/10.1109/34.908964

[20] Liu, Z., Shan, Y. and Zhang, Z. (2001) Expressive Expression Mapping with Ratio Images. *Proceedings of the* 28*th Annual Conference on Computer Graphics and Interactive Techniques*, Los Angeles, 12-17 August 2001, 271-276. https://doi.org/10.1145/383259.383289

[21] Yu, H. and Wang, G. (2010) A Soft-Threshold Filtering Approach for Reconstruction from a Limited Number of Projections. *Physics in Medicine and Biology*, **55**, 3905-3916. https://doi.org/10.1088/0031-9155/55/13/022

[22] Yu, W., Wang, C., Nie, X., Huang, M. and Wu, L. (2017) Image Reconstruction for Few-View Computed Tomography Based on ℓ0 Sparse Regularization. *Procedia Computer Science*, **107**, 808-813. https://doi.org/10.1016/j.procs.2017.03.178

[23] Ji, D., Qu, G. and Liu, B. (2016) Simultaneous Algebraic Reconstruction Technique Based on Guided Image Filtering. *Optics Express*, **24**, Article No. 15897. https://doi.org/10.1364/oe.24.015897

[24] Wang, Z., Bovik, A.C., Sheikh, H.R. and Simoncelli, E.P. (2004) Image Quality Assessment: From Error Visibility to Structural Similarity. *IEEE Transactions on Image Processing*, **13**, 600-612. https://doi.org/10.1109/tip.2003.819861

[25] Storath, M., Weinmann, A., Frikel, J. and Unser, M. (2015) Joint Image Reconstruction and Segmentation Using the Potts Model. *Inverse Problems*, **31**, Article ID: 025003. https://doi.org/10.1088/0266-5611/31/2/025003

[26] Tang, K., Yang, J. and Wang, J. (2014) Investigating Haze-Relevant Features in a Learning Framework for Image Dehazing. 2014 *IEEE Conference on Computer Vision and Pattern Recognition*, Columbus, 23-28 June 2014, 2995-3002. https://doi.org/10.1109/cvpr.2014.383